Chapter 4
Complementary Use of Electron Cryomicroscopy and X-Ray Crystallography: Structural Studies of Actin and Actomyosin Filaments

Takashi Fujii and Keiichi Namba

Abstract Visualization of macromolecular structures is essential for understanding the mechanisms of biological functions because they are all determined by the structure and dynamics of macromolecular complexes. Electron cryomicroscopy (cryoEM) and image analysis has become a powerful tool for structural studies because of recent technical developments in microscope optics, cryostage control, image detection and the methods of sample preparation. In particular, the recent development of CMOS-based direct electron detectors with high sensitivity, high resolution and high frame rate has revolutionized the field of structural biology by making near-atomic resolution structural analysis possible from small amounts of solution samples. However, for some biological systems, it is still difficult to reach high resolution due to somewhat flexible nature of the structure, and a complementary use of cryoEM with X-ray crystallography is essential and useful to gain mechanistic understanding of the biological functions and mechanisms. We will describe our strategy for the structural analyses of actin filament and actomyosin rigor complex and the biological insights we gained from these structures.

Keywords Hybrid method for structural analysis · Electron cryomicroscopy · Image analysis · 3D reconstruction · X-ray crystallography · F-actin assembly · Treadmill · Actomyosin motor · Skeletal muscle contraction · Biased Brownian motion

T. Fujii · K. Namba (✉)
Graduate School of Frontier Biosciences, Osaka University, Suita, Osaka, Japan

Quantitative Biology Center, Riken, Osaka, Japan
e-mail: keiichi@fbs.osaka-u.ac.jp

H. Nakamura et al. (eds.), *Integrative Structural Biology with Hybrid Methods*,
Advances in Experimental Medicine and Biology 1105,
https://doi.org/10.1007/978-981-13-2200-6_4

4.1 Introduction

Biological functions and activities that support the life of every biological organism are diverse, and yet the basic mechanisms that determine and exert those biological functions are highly shared by diverse organisms, from microorganisms such as bacteria and yeast to multicellular organisms such as animals and plants. Even the complex human brain functions are not the exception. The basic mechanisms are highly shared because all these functions are designed and determined by the structures of proteins and nucleic acids with complex three-dimensional (3D) arrangements of so many atoms that comprise these molecules, with the number ranging from a few to tens and hundreds of thousands. Moreover, their structures are not solid unlike bulk materials of metals and ceramics but are very dynamic and flexible so that they can function by actively utilizing thermal fluctuations. One of the major challenges in life science is the elucidation of mechanisms that determine and exert these extremely diverse functions by looking into the 3D structures and dynamics of so many different biological macromolecules involved in those diverse biological functions. We also need to look at the structures of macromolecules in each of their functional states appearing in the entire process of their functional cycles. Therefore the number of 3D structures we need to solve would be extremely large, probably ranging at least from a few hundreds of thousands to a few million.

Thus, structural information of biological macromolecular machinery is essential for understanding the mechanisms by which they function, and various methods for structural analyses have been developed to obtain structural information at highest possible resolution. We have been studying the structures and functions of protein motor complexes, such as the bacterial flagellar motor and actomyosin, to understand the mechanisms of force generation and highly efficient energy conversion. We have developed various techniques in X-ray fiber diffraction, X-ray crystallography and electron cryomicroscopy (cryoEM) and used them in a complementary manner to build atomic models of the motor complexes by docking crystal structures of component proteins into 3D density maps obtained by X-ray fiber diffraction and/or cryoEM and refining the entire models against these maps (Namba et al. 1985; Namba and Stubbs 1985, 1986; Samatey et al. 2001, 2004; Yonekura et al. 2003; Fujii et al. 2009, 2010; Gayathri et al. 2012; Fujii and Namba 2017). Although cryoEM image analysis has become a powerful tool for the structural analysis of macromolecular complexes by the recent introduction of direct electron detecting CMOS cameras and is now capable of resolving the structures at near atomic detail to allow *de novo* atomic model building as described in the following section, there are still many cases where the resolution is limited by the flexible and/or dynamic nature of the specimens, and a complementary use of cryoEM for the entire complex and X-ray crystallography or NMR of component molecules is necessary and useful to build the entire atomic model to study the structure-function relationships in such cases. We will describe a few example cases to demonstrate the usefulness of the method.

4.2 Power of cryoEM Image Analysis in the Past and Present

CryoEM image analysis, especially single particle image analysis, is a potentially powerful method because there is no need for sample crystallization that is essential for X-ray crystallography and there is virtually no upper limit in the size of molecular complexes unlike NMR. The structures of macromolecular complexes can be directly visualized by cryoEM in various functional states. It would therefore be desirable that cryoEM can visualize the structures of the macromolecular complexes at atomic resolution. The 2017 Nobel Prize in Chemistry was awarded to Jacques Dubochet (University of Lausanne, Switzerland), Joachim Frank (Columbia University, USA), and Richard Henderson (MRC Laboratory of Molecular Biology, UK), for their pioneering works in 1970s and 1980s in the development of cryoEM image analysis techniques for the structural analysis of biological macromolecules. By the development of transmission electron cryomicroscopes (cryoTEM) over many years in 1980s and 90's, especially those done in Japan, such as the implementation of a liquid helium-cooled specimen stage to minimize the radiation damage (Fujiyoshi et al. 1991) and a field emission electron gun to use a highly-coherent electron beam (Mimori et al. 1995), as well as various improvements in the method of image analysis, it became possible to achieve near atomic resolution for 2D crystal structures of membrane proteins, such as bacteriorhodopsin and aquaporin (Kimura et al. 1997; Mitsuoka et al. 1999; Murata et al. 2000) and filamentous helical assemblies of proteins, such as the bacterial flagellar filament (Yonekura et al. 2003). It was encouraging to see the polypeptide backbone folding and large side chains of flagellin clearly resolved in the structure of the bacterial flagellar filament at around 4 Å resolution analyzed from a set of filament images corresponding to only 40,000 flagellin molecules. Since the image quality and signal to noise ratio (S/N) of frozen-hydrated biological macromolecules embedded in vitreous ice is quite poor due to an extremely low electron dose to avoid radiation damage, a high cryo-protection factor by lowering the specimen temperature down to 4 K by liquid helium gave us a substantial advantage for achieving unprecedented resolution. However, it was by no means a high-throughput work partly because we had to use photographic films as the image detector.

By further implementation of new technologies in cryoTEM in 2000s, such as the CCD camera to evaluate the image quality immediately after recording by Fourier transformation and in-column energy filter to eliminate inelastically scattered electrons that form a high background noise, and working at a slightly elevated specimen temperature to around 50 K to increase the electron conductivity of the ice embedded specimen to reduce its charge up that tends to blur the cryoEM images, the efficiency of high-quality image data collection was drastically improved, and the image analysis by the computer became much faster by the improvement in the software and semiconductor nanotechnologies. These improvements made previously several years of works be done within a few weeks, and the visualization of protein secondary structures became relatively easy and quick (Fujii et al. 2009; Fujii et al. 2010; Gayathri et al. 2012), demonstrating a potential of achieving near

atomic resolution within such a short period of time as far as the structure is well ordered and stable, such as tobacco mosaic virus.

Then, at the end of 2013, two milestone papers were published by Yifan Cheng and his colleagues on the structure of the TRPV1 receptor ion channel, a membrane receptor protein that responds to heat and spiciness, solved at 3.4 Å resolution by cryoEM image analysis of about 100,000 single particle images of the protein picked up from about 1000 cryoEM images obtained from a small amount of sample solution (Liao et al. 2013; Cao et al. 2013). They were involved in the development of a CMOS-based direct electron detector camera and fully utilized its capability to record images of 4 K × 4 K pixels at 400 frames per second to carry out single electron counting to minimize the detection noise called the Landau noise, which is an intrinsic noise of large distribution that any types of energy accumulating detectors, such as film and CCD, suffer for individual electron detection. They also devised a way to collect sharp high-quality cryoEM images of proteins by movie-mode imaging and motion correction to minimize the image blur caused by a mechanical drift of the specimen stage and the distortion of ice film caused by electron irradiation (Li et al. 2013). Together with the development of a user-friendly, yet sophisticated image analysis software package, RELION (Scheres 2012; Kimanius et al. 2016), cryoEM image analysis has now become a very powerful tool for structural biology, achieving near atomic resolution in the structural analysis of many different macromolecular complexes including membrane proteins to allow *de novo* atomic model building relatively easily.

However, there are still many cases where the resolution is limited by the flexible and/or dynamic nature of the specimens, and in such cases a complementary use of cryoEM for the entire complex and X-ray crystallography or NMR of component molecules is necessary and useful to study the structure-function relationships. We will describe our structural studies of the skeletal muscle F-actin and actomyosin complex to demonstrate the usefulness of the complementary method.

4.3 Structural Study of F-Actin

F-actin is a helical assembly of actin, is an essential component of muscle fibers for contraction and also plays crucial roles in various cellular processes as the most abundant component and regulator of cytoskeletons by dynamic assembly and disassembly processes (from G-actin to F-actin and vice versa), such as those called lamellipodia and filopodia (Pollard and Borisy 2003; Carlier and Pantaloni 2007). While actin is a ubiquitous protein and is involved in the various important biological functions and many crystal structures of actin were available over the years since the first crystal structure in complex with DNase-I (Kabsch et al. 1990), the definitive high-resolution structure of F-actin remained unknown until 2010 (Fujii et al. 2010). Steady technical advances in cryoEM image analysis over the years allowed near-atomic resolution structural analyses of many icosahedral viruses and helical assembly of macromolecules, such as the bacterial flagellar

filament, the tubular crystal of acetylcholine receptor and tobacco mosaic virus (TMV) in 2000s (Yonekura et al. 2003; Miyazawa et al. 2003; Sachse et al. 2007). But, it was possible to reach such high resolutions even by using photographic films as image detectors simply because their particle sizes or diameters were large enough to produce sufficiently high image contrast and S/N in their cryoEM images of ice-embedded frozen-hydrated specimens that allows accurate alignment and average of many particle images necessary to recover high-resolution structural information hidden under the noise. Since F-actin is a relatively thin filament with a flexible, twisted ribbon-like structure with the maximum diameter of only 10 nm, which is far thinner than TMV (18 nm) or the flagellar filament (23 nm), the image contrast of unstained, frozen-hydrated specimen is extremely low, making accurate image alignment extremely difficult and thereby high-resolution structural analysis elusive.

We used a cryoTEM (JEOL JEM-3200FSC) equipped with a field emission electron gun, a liquid helium-cooled specimen stage, an in-column Ω-type energy filter, and a CCD camera (TIPVS F415MP) to collect cryoEM images of F-actin. We were able to obtain a remarkable gain (∼5 times) in image contrast by the use of energy filtering, by controlling ice thickness, and by recording images at a specimen temperature of 50 K instead of 4 K (Fujii et al. 2009). Such improvement in image contrast allowed us to see the two-stranded helical features of F-actin in raw cryoEM images even at relatively small defocus levels close to 1 μm (Fig. 4.1). Image recording by a CCD camera made high-quality data collection remarkably efficient. To avoid undesirable dumping of high-resolution contrast by a poor modulation transfer function of the CCD camera, we used a relatively high magnification of approximately 172,000× (0.87 Å/pixel). We collected 490 cryoEM images manually in two days, picked up filament images and used a single particle image analysis method but still utilized the helical symmetry to make the image alignment as accurate as possible (Sachse et al. 2007; Fujii et al. 2009; Egelman

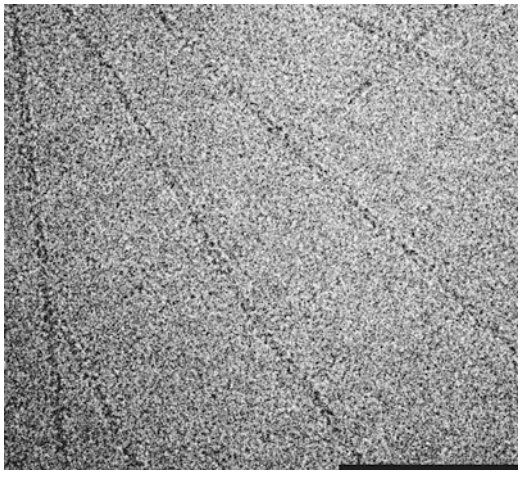

Fig. 4.1 CryoEM image of F-actin in a frozen hydrated state recorded by CCD under a defocus value of 1500 nm. Scale bar, 100 nm

2000). Since the image analysis procedure was fully automated, it was completed within 2 days to reconstruct the final 3D image, and the resolution was 6.6 Å (at the Fourier shell correlation (FSC) = 0.143) (EMD-5168) (Fujii et al. 2010).

The resolution of the 3D map was high enough to clearly visualize the secondary structures, such as α-helices, β-sheets and β-hairpins, and even some loops and the extended N-terminal chain that had never been seen in the crystal structures clearly showed up. So it was possible to build a complete atomic model of F-actin far more reliably than before. It was debated over long time that F-actin must have an intrinsic flexibility in its helical order and that is why the structures solved by cryoEM image analysis were limited to low resolution, but the fact that such a high resolution was achieved as described above by using over 90% of the image data we collected indicates that the flexibility is not so high as the previous studies suggested (Galkin et al. 2008).

To build an atomic model of F-actin, we employed a program FlexEM (Topf et al. 2008), which refines the atomic model while fitting it into the EM density map by simulated annealing molecular dynamics with stereochemical and non-bonded interaction terms restrained. We used the crystal structure of uncomplexed actin (PDB code: 1J6Z) (Otterbein et al. 2001) as an initial model and divided it into four domains D1, D2, D3 and D4 to treat them as independent units because these four domains have well-defined hydrophobic cores. In the initial stage of the fitting process, we treated them as rigid bodies and allowed the joints of these domains to be flexible, but residues 1–8, 39–56, 221–234 and 337–375 were outside the density map. In the second stage, we allowed these residues to move flexibly to fit into the map under stereochemical restraints and then applied the helical symmetry of F-actin to this subunit model to build a complete F-actin model. We then minimized the conformational energy further by FlexEM to remove intermolecular clashes of atoms. The processes of the fitting and refinement are shown in Fig. 4.2, and the final refined model in Fig. 4.3 (PDB: 3FMP) (Fujii et al. 2010). The conformation of domains 1, 3 and 4 did not change so largely as indicated by the relatively small root-mean-squares (rms) displacements of Cα atoms (domain 1: 0.3 Å; domain 3: 0.3 Å; domain 4: 0.8 Å). This is consistent with the fact that these three domains have stable conformations with well-defined hydrophobic cores and assures the reliability of the atomic model as well as the high quality of the cryoEM map. Domain 2 was, however, an exception. The 2-turn short α-helix (residues 40–48) at the tip of the D-loop (the DNase I binding loop) in the actin crystal structure (Otterbein et al. 2001) became an extended loop (residues 38–53), reaching the bottom pocket between domains D1 and D4 of the above actin subunit (Fig. 4.3). Such a conformational change had been predicted from its variable conformations in the crystal structures of actin and its possible involvement in the axial intersubunit interactions (Oda et al. 2009), but this D-loop conformation was unique, indicating that it is totally dependent upon the molecule that it binds to.

Since the nature of conformational change from G-actin to F-actin is of immense importance for biological implications for actin functions, we carefully compared the F-actin structure with the crystal structure of G-actin. While the two major-domains were twisted in the crystal structures, they became flat in the F-actin

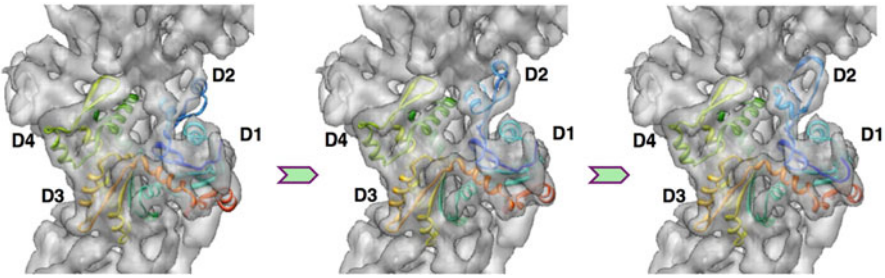

Fig. 4.2 Process of docking and refinement of actin atomic model in the cryoEM density map from left to right. Four domains of actin are labeled D1, D2, D3 and D4. Left, G-actin crystal structure, presented as a Cα ribbon diagram, is docked into the cryoEM density map as a rigid body. Each domain is not well fitted to the density. Middle, each of the four domains is independently moved and rotated as a rigid body to fit to the density map. Domain D2 is still not fitted well. Right, the conformation of each domain is refined against the density map by flexible fitting

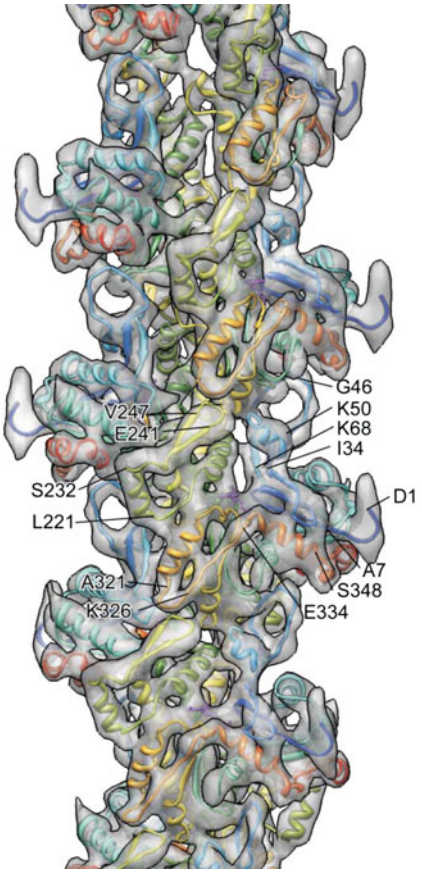

Fig. 4.3 CryoEM density map of F-actin (EMD-5168) with a fitted and refined atomic model (PDB: 3MFP) (Fujii et al. 2010). The model is presented as a Cα ribbon diagram colored in rainbow from the N-terminus in blue to the C-terminus in red. Approximately seven subunits of actin are shown. Some amino acid residues are labeled as a guild to follow the chain

model in a similar manner to the relative domain motions described previously for the model that nicely reproduced X-ray fiber diffraction intensity data obtained from a highly oriented liquid-crystalline sol specimen of F-actin (Oda et al. 2009). However, the relative domain motions were more complex than those described previously. Together with the conformational change of the D-loop, these changes made the slightly bent domains 1–2 in G-actin significantly flatter in F-actin, allowing the D-loop to reach and bind to the bottom pocket between domains D1 and D4 of the above actin subunit. This is how the axial intersubunit interactions along the protofilament are made tight for F-actin polymerization as shown in Fig. 4.3. Including the interactions between protofilaments, the nature of intersubunit interactions between actin subunits is mostly electrostatic or hydrophilic, and this explains depolymerization of F-actin at concentrated salt solutions (Nagy and Jencks 1965).

Actin polymerization is known to have a distinct polarity, showing fast polymerization at the barbed end of F-actin while slow depolymerization from the pointed end under certain conditions (Fujiwara et al. 2007). This is called treadmilling and plays important roles in the formation of lamellipodia and filopodia for cell motility and morphogenesis (Pollard and Borisy 2003; Carlier and Pantaloni 2007). The conformational changes of actin between its monomeric G-actin form and polymerized F-actin form explains how this asymmetry is achieved (Fig. 4.4). Actin

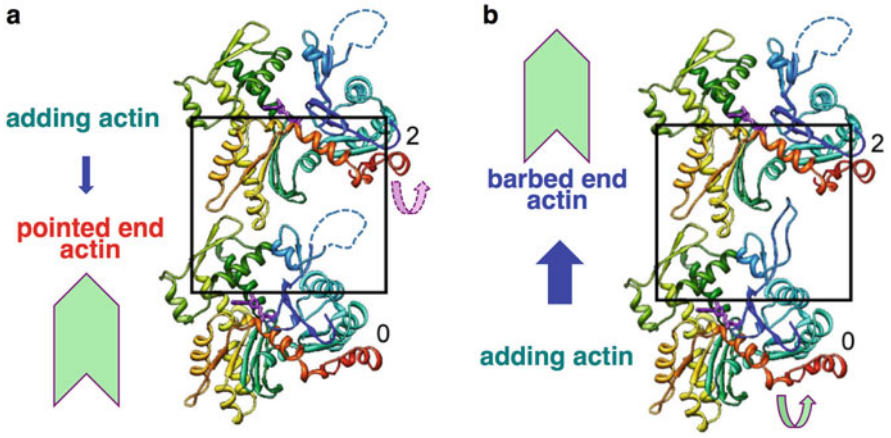

Fig. 4.4 Structural asymmetry of F-actin responsible for the difference in the assembly kinetics at the pointed and barbed ends. (**a**) An actin subunit shown above is being added to the pointed end of F-actin shown below. The flexible D-loop of actin at the pointed end is presented by dashed line. The domain motion of adding actin occurs but its F-actin conformation cannot be stabilized, as indicated by purple dashed arrow, due to the flexible D-loop of actin at the pointed end. (**b**) An actin subunit shown below is being added to the barbed end of F-actin show above. Because the bottom pocked of actin at the barbed end is well ordered and has a stable F-actin conformation to act as the template for actin assembly, the D-loop of adding actin binds to the pocket and is stabilized to make the entire adding actin conformation stable in the F-actin form after domain motion, as indicated by green solid arrow

at the barbed end is stably in the F-actin conformation, forming the bottom pocket for the binding of actin subunit in the G form. The structure of the bottom pocket acts as the template for the formation of the D-loop with the above mentioned domain motions of adding actin to turn it into the F form, and this facilitates the polymerization of actin. On the other hand, because actin at the pointed end has domain D2 exposed to solution, the D-loop conformation cannot stabilized at all. The exposed D-loop of domain D2 must be flexible and dynamic to make the binding of adding actin rather difficult because adding actin also has to change its conformation from the G to F form in order to bind to F-actin but no stable template structure is available for these conformational changes to occur and be stabilized. Thus, the asymmetry in the structure and conformational dynamics of actin at the barbed and pointed ends of F-actin is responsible for the distinct difference in the polymerization kinetics of actin at the both ends. The complementary use of cryoEM and X-ray crystallography allowed us to gain deep insights into this biologically important mechanism.

4.4 Structural Study of Skeletal Muscle Actomyosin Rigor Complex

Muscle contraction occurs by mutual sliding of thick myosin filaments and thin actin filaments that shortens sarcomeres, the contractile units that regularly repeat along the entire muscle cells (Huxley 1969). The sliding force is generated via cyclic interactions of myosin heads, which are periodically projecting out from the thick filament towards surrounding thin actin filaments, with actin molecules of the thin filaments. Myosin head is an ATPase, and its ATP binding and hydrolysis regulates the cyclic association and dissociation of myosin with actin filament (Lymn and Taylor 1971). Upon binding of MgATP, myosin hydrolyses ATP relatively quickly but the hydrolysis products ADP and Pi stay in the nucleotide-binding pocket, and therefore its ATPase cycle does not proceed until myosin head binds to actin filament. Therefore, a conformational change of myosin head must occur upon binding to actin filament, and this should be responsible for this actin-activated ATPase, but structural information on the actomyosin rigor complex was limited to reveal this mechanism. X-ray crystal structures of the head domains of various myosins, such as myosin II, V and VI, in different nucleotide-binding states have suggested that myosin undergoes conformational changes during ATPase cycle in its lever arm domain to be in largely different angles within the plain of actin filament axis and that such changes represent a power stroke that drives the unidirectional movement of myosin against actin filament (Holmes et al. 2004; Sweeney and Houdusse 2004). However, since those myosin head structures obtained in atomic details were all in the absence of actin filament (Rayment et al. 1993; Dominguez et al. 1998; Bauer et al. 2000; Houdusse et al. 2000; Coureux et al. 2003; Reubold

et al. 2003, 2005; Ménétry et al. 2005, 2008; Yang et al. 2007), key piece of information was still missing.

The structure of the actomyosin rigor complex had been analyzed by electron cryomicroscopy (cryoEM) and image analysis (Holmes et al. 2003; Behrmann et al. 2012). However, the resolution and quality of the density maps were limited to reveal the conformational changes in sufficient detail, and it was still not so clear how ADP and Pi are released upon strong binding of myosin to actin filament and how ATP binding to myosin causes its dissociation from actin filament. We therefore solved the structure of actomyosin rigor complex of rabbit skeletal muscle by cryoEM image analysis. We obtained a 3D density map at 5.2 Å resolution (EMD-6664) and built an atomic model (PDB: 5H53) by using a method similar to that we used for F-actin as described in the previous section (Fig. 4.5) (Fujii and Namba 2017). We used the crystal structure of squid muscle myosin S1 fragment in the rigor-like state (PDB: 3I5G) (Yang et al. 2007) and the cryoEM structure of skeletal muscle F-actin (PDB: 3MFP) (Fujii et al. 2010) for docking and refinement. We employed DireX (Schroder et al. 2007) and FlexEM (Topf et al. 2008) to refine these models by flexible fitting while preserving stereochemistry. We carried out this model fitting refinement carefully to avoid overfitting, by imposing a relatively strong restraint to keep the conformations of individual domains with independent hydrophobic cores unchanged as much as possible and trying not to fit individual secondary structure elements separately. As a reliability measure of our model, the rms deviations of Cα atoms for individual domains of myosin head of our rigor model from those of a crystal rigor-like model (PDB: 3I5G) (Yang et al. 2007) were calculated, and they were all with a range from 1.0 to 1.6 Å, which was comparable to those between crystal structures of myosin in different conformations, assuring that our model was refined without over fitting.

We then compared this structure with those of myosin in different nucleotide-binding states solved by X-ray crystallography and found a distinctly large conformational change of myosin head that widely opens up the nucleotide-binding pocket, even compared with the rigor-like structures of myosin head without nucleotide in the pocket (Fig. 4.6). It was obvious that this conformational change allows ADP and Pi to be quickly released from their binding sites upon myosin binding to actin filament. Myosin has been called a backdoor enzyme (Yount et al. 2007) because Pi leaves before ADP (Geeves et al. 1984) and a possible pathway for Pi release has been found only in the backside of the pocket in the myosin crystal structures (Yang et al. 2007; Llinas et al. 2015). However, the structure of actomyosin rigor state with such a widely open pocket (Fig. 4.6) suggests that Pi is likely to be released also from the front side. Although it is not obvious why Pi leaves before ADP, electrostatic repulsion by the negative charges of Pi or the way the ADP moiety is tightly bound by myosin may be responsible for this.

Recent publications on the structures of actomyosin rigor complexes by cryoEM image analysis revealed the structures of cytoplasmic myosins or smooth muscle myosin strongly bound to actin filament (von der Ecken et al. 2016; Wulf et al. 2016; Banerjee et al. 2017; Mentes et al. 2018). They all show a similar conformational change of myosin head to those we observed for skeletal muscle myosin albeit in

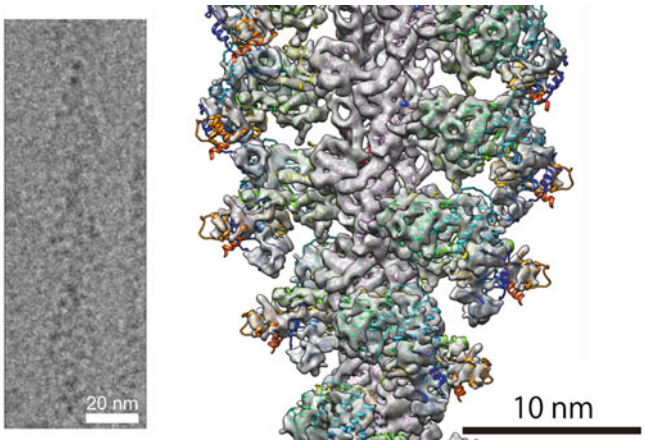

Fig. 4.5 CryoEM image and the reconstructed density map of actomyosin rigor complex (EMD-6664) with the model of actin and myosin after docking and refinement (PDB: 5H53) (Fujii and Namba 2017). The cryoEM image shows the typical arrowhead feature of the complex. About nine subunits of actin and myosin head are presented. Ribbon models of actin are colored purple and myosin in rainbow according to the sequence

much less extent, and those structures share the conformations with those of the crystal rigor-like structures with much less open nucleotide binding pocket that does not allow such a quick release of ADP and Pi as skeletal muscle myosin in the rigor state. The rates of ATP hydrolysis cycle of cytoplasmic and smooth muscle myosins are actually much slower than that of skeletal muscle myosin, and the same is true for the speed of myosin movement along actin filament. It appears that the structures of different types of myosins are optimally designed to move along actin filament at different speeds required for their physiological functions, and the rate of chemo-mechanical cycle is determined differently by their similar but distinct level of conformational changes.

Structural comparison of our rigor model with an ATP bound post-rigor structure (Rayment et al. 1993) revealed how ATP binding may trigger dissociation of myosin from actin filament. We superposed myosin L50D domain (N473 – A593), which contains the helix-loop-helix tightly attached to two neighboring actin molecules along the protofilament (Fig. 4.7), to see what would occur in the actomyosin interactions upon ATP binding. We used L50D for superposition because this domain occupies the largest area of actomyosin interface. In the rigor structure, the CM loop and loop 4 are nicely fitted on and tightly bound to actin surface (domains D1 and D3, Fig. 4.7 top panel), but the post-rigor structure thus superimposed on the rigor structure shows a serious steric clash of the CM loop with domain D1 of actin (Fig. 4.7 middle panel). This clash is caused by U50D rotation nearly as a rigid body by 21° around the long axis of myosin head and appears to be the main cause of myosin dissociation from actin filament upon ATP binding. Assuming that L50D and loop 2 stay bound to both actin subunits with hydrophobic and electrostatic

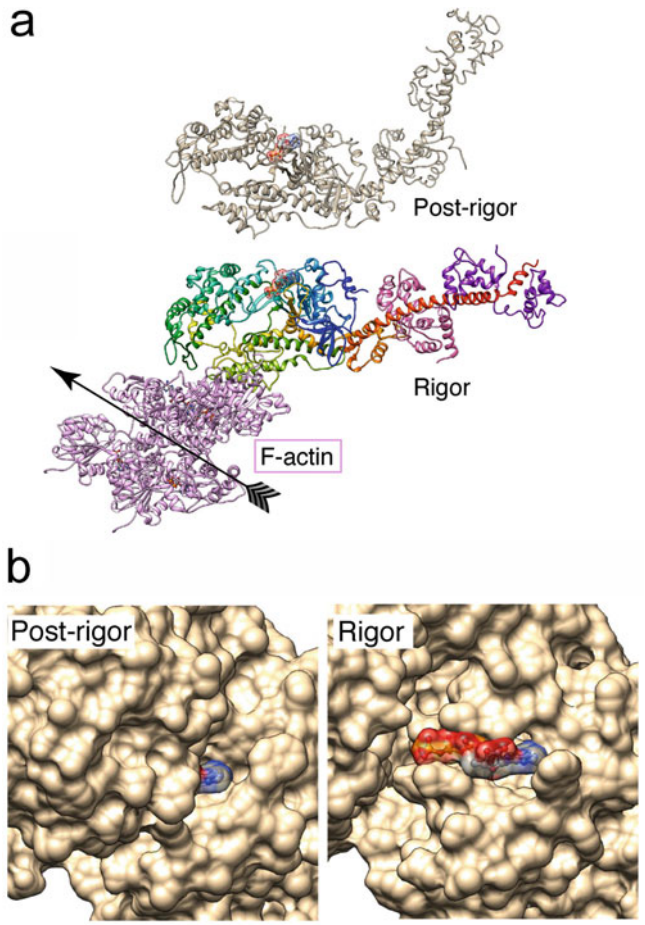

Fig. 4.6 Comparison of myosin structures in the actomyosin rigor state and a post-rigor state. (**a**) The post-rigor crystal structure of chicken muscle myosin (PDB: 2MYS) (Rayment et al. 1993) and the actomyosin rigor complex (PDB: 5H53) (Fujii and Namba 2017), viewed nearly in the axial direction of the filament from its barbed end. ATP is included in both models to indicate its binding position. (**b**) The nucleotide-binding sites of the two models in solid surface representation showing how widely the nucleotide-binding pocket is open when myosin head is bound strongly to actin filament in the rigor state

interactions, respectively, this CM loop clash against actin would push the CM loop back and cause a clockwise rotation of the entire motor domain by about 20° around its long axis to avoid the clash, and this results in a significant reduction in the interface area between myosin and two actin subunits to destabilize the actomyosin interactions (Fig. 4.7 bottom panel). This model would represent a possible structure of actomyosin in the weak binding state formed upon ATP binding, and this would be the state of myosin ready to dissociate from actin filament.

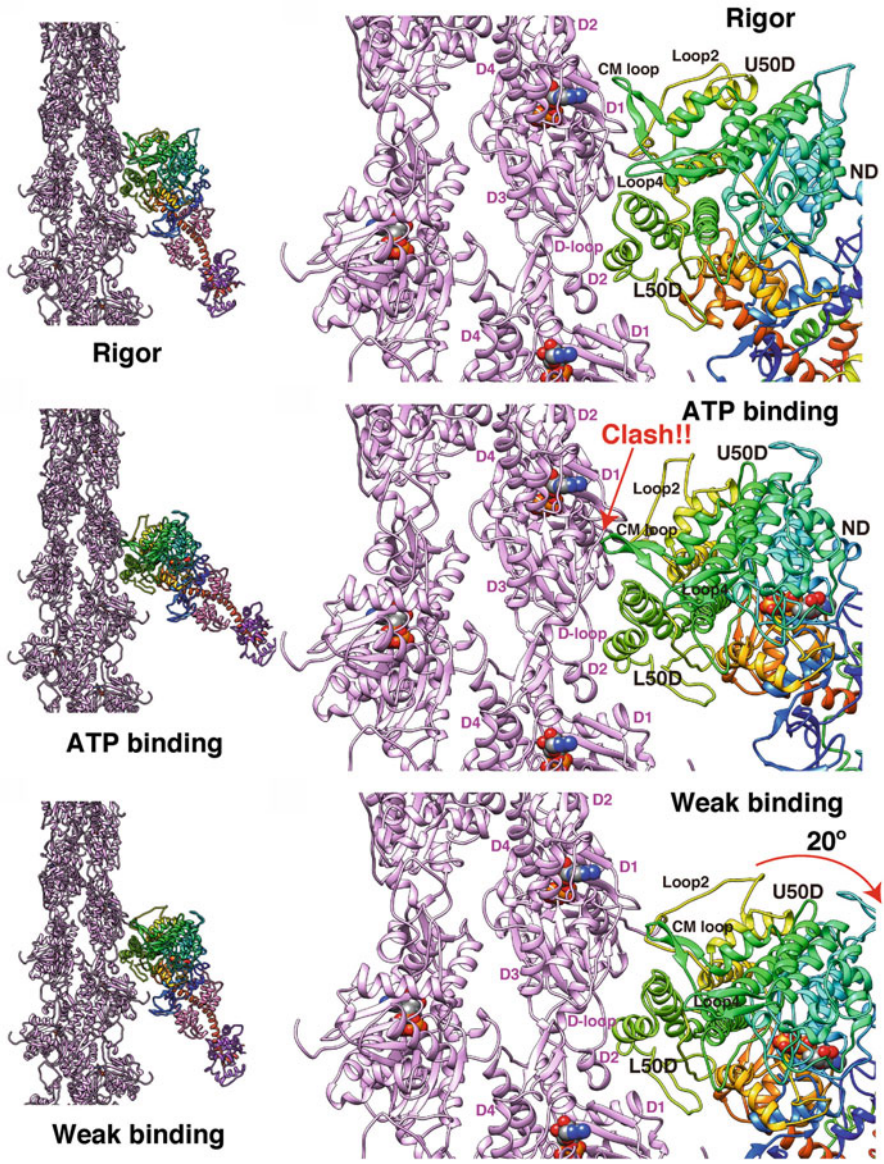

Fig. 4.7 Conformational changes of rigor myosin head upon ATP binding and its possible consequence to form the weak binding state. Top panel shows the actomyosin rigor structure. The middle panel shows the myosin structure upon ATP binding with its L50D helix-loop-helix and loop 2 still attached to actin. The bottom shows myosin head after rotation to avoid the clash of CM loop with actin where L50D helix-loop-helix and loop 2 still attached to actin. Left panels are overviews, and the right panels are magnified. The N-terminal portion of loop 2 must be flexible enough to allow myosin head rotation while the lysine-rich C-terminal portion stays attached to the N-terminal region of actin to keep electrostatic interactions of the weak binding state. The crystal structure of chicken muscle myosin in the post-rigor state (PDB: 2MYS) was used to build the models shown in the middle and bottom panels by including loop 2 in different conformations to accommodate different distances between actin D1 and myosin U50D

A preferential binding of myosin to actin filament has been observed depending on the direction of relative motion and/or force (Iwaki et al. 2009). The asymmetry in the putative model of weakly bound actomyosin (Fig. 4.7, and schematically depicted in Fig. 4.8) can explain how such directionally preferential binding can be achieved. This structural asymmetry can also cause directionally preferential release of myosin upon ATP binding from actin filament, and the probability of dissociation is higher when actin filament moves forward to its pointed end than when actin filament moves backward to its barbed end. So the unidirectional sliding motions of myosin and actin filament could be achieved by just biasing their relative Brownian motions within each sarcomere by this directionally preferential release of myosin. This thermal-driven mechanism can explain why the sliding distance of myosin and actin filament in sarcomere is longer than 60 nm per one ATP hydrolysis cycle (Yanagida et al. 1985), which is much longer than the one predicted by the power stroke of myosin lever arm, and how a single myosin head can go through multiple steps of 5.3 nm along actin filament until myosin head strongly binds to actin by release of ADP and Pi when myosin is forced to stay near actin filament (Kitamura et al. 1999). These rather intriguing observations suggested the presence and involvement of a biased Brownian motion in the actomyosin motility mechanism, but how it can be achieved was elusive until we saw the molecular structures in detail. Thus, the complementary use of cryoEM and X-ray crystallography again played a very important role in revealing this biologically important mechanism.

Fig. 4.8 Schematic diagram of actomyosin structure in the weak binding state, showing a possible mechanism of preferential transition to the strong binding state in the backward movement of actin filament (downward in this figure) and preferential release of myosin head from actin filament in the forward movement of actin filament (upward in this figure). Clockwise rotation of myosin by upward movement of actin filament (middle to bottom) can occur more easily than counterclockwise rotation by downward movement (middle to top), because the bonds between myosin and two actin subunits can be broken one after another by clockwise rotation, starting from those on the tip of CM loop (middle to bottom) but the tip of CM loop becomes the center or fulcrum of rotation by counterclockwise rotation and therefore many bonds between L50D and two actin subunits have to be broken simultaneously (middle to top). This results in a longer lifetime of the weak binding state, thereby a higher probability of transition to the strong binding state in the backward (downward) movement of actin filament and also in a directionally preferential release of myosin head in the forward movement of actin filament, causing a biased Brownian motion. Blue arrows indicate the directions of actin filament movement and myosin rotation, and dashed black arrows indicate the probabilities of transitions between the states by their sizes

Fig. 4.8 (continued)

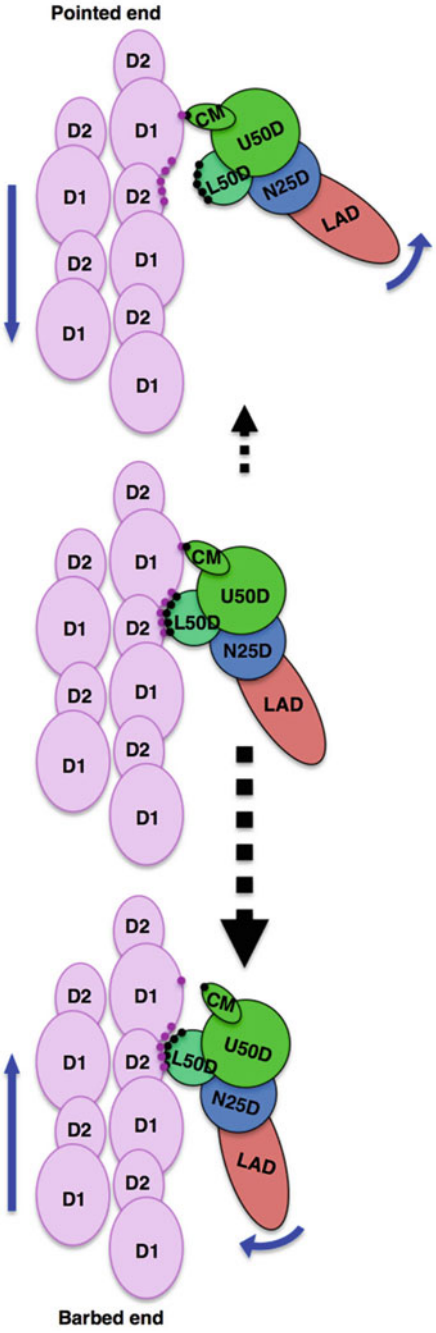

Acknowledgement This work was supported by JSPS KAKENHI Grant number 25711010 to T.F and 25000013 to K.N.

References

Banerjee C, Hu Z, Huang Z, Warrington JA, Taylor DW, Trybus KM, Lowey S, Taylor KA (2017) The structure of the actin-smooth muscle myosin motor domain complex in the rigor state. J Struct Biol 200:325–333

Bauer CB, Holden HM, Thoden JB, Smith R, Rayment I (2000) X-ray Structures of the Apo and MgATP-bound States of Dictyostelium discoideum Myosin Motor Domain. J Biol Chem 275:38494–38499

Behrmann E, Müller M, Penczek PA, Manherz HG, Manstein D, Raunser S (2012) Structure of the rigor actin-tropomyosin-myosin complex. Cell 150:327–338

Cao E, Liao M, Cheng Y, Julius D (2013) TRPV1 structures in distinct conformations reveal activation mechanisms. Nature 504:113–118

Carlier MF, Pantaloni D (2007) Control of actin assembly dynamics in cell motility. J Biol Chem 282:23005–23009

Coureux PD, Wells AL, Ménétry J, Yengo CM, Morris CA, Sweeney HL, Houdusse A (2003) A structural state of the myosin V motor without bound nucleotide. Nature 425:419–423

Dominguez R, Freyzon Y, Trybus KM, Cohen C (1998) Crystal structure of a vertebrate smooth muscle myosin motor domain and its complex with the essential light chain: visualization of the pre-power stroke state. Cell 94:559–571

Egelman EH (2000) A robust algorithm for the reconstruction of helical filaments using single-particle methods. Ultramicroscopy 85:453–463

Fujii T, Namba K (2017) Structure of actomyosin rigour complex at 5.2 Å resolution and insights into the ATPase cycle mechanism. Nature Commun 8:13969 (11pp)

Fujii T, Kato T, Namba K (2009) Specific arrangement of α-helical coiled coils in the core domain of the bacterial flagellar hook for the universal joint function. Structure 17:1485–1493

Fujii T, Iwane AH, Yanagida T, Namba K (2010) Direct visualization of secondary structures of F-actin by electron cryomicroscopy. Nature 467:724–728

Fujiwara I, Vavylonis D, Pollard TD (2007) Polymerization kinetics of ADP- and ADP-Pi-actin determined by fluorescence microscopy. Proc Natl Acad Sci U S A 104:8827–8832

Fujiyoshi Y, Mizusaki T, Morikawa K, Yamagishi H, Aoki Y, Kihara H, Harada Y (1991) Development of a superfluid helium stage for high-resolution electron microscopy. Ultramicroscopy 38:241–251

Galkin VE, Orlova A, Cherepanova O, Lebart MC, Egelman EH (2008) High-resolution cryo-EM structure of the F-actin-fimbrin/plastin ABD2 complex. Proc Natl Acad Sci U S A 105:1494–1498

Gayathri P, Fujii T, Møller-Jensen J, van den Ent F, Namba K, Löwe J (2012) A bipolar spindle of antiparallel ParM filaments drives bacterial plasmid segregation. Science 338:1334–1337

Geeves MA, Goody RS, Gutfround H (1984) Kinetics of acto-S1 interaction as a guide to a model of the crossbridge cycle. J Muscle Res Cell Motil 5:351–356

Holmes KC, Angert I, Kull FJ, Jahn W, Schröder RR (2003) Electron cryo-microscopy shows how strong binding of myosin to actin releases nucleotide. Nature 425:423–427

Holmes KC, Schroder RR, Sweeney HL, Houdusse A (2004) The structure of the rigor complex and its implications for the power stroke. Philos Trans R Soc B 359:1819–1828

Houdusse A, Szent-Gyögyi AG, Cohen C (2000) Three conformatinoal states of scallop myosin S1. Proc Natl Acad Sci U S A 97:11238–11243

Huxley HE (1969) The mechanism of muscular contraction. Science 164:1356–1365

Iwaki M, Iwane AH, Shimokawa T, Cooke R, Yanagida T (2009) Brownian search-and-catch mechanism for myosin-VI steps. Nature Chem Biol 5:403–405

Kabsch W, Mannherz HG, Suck D, Pai EF, Holmes KC (1990) Atomic model of the actin:DNase I complex. Nature 347:37–44

Kimanius D, Forsberg BO, Scheres SH, Lindahl E (2016) Accelerated cryo-EM structure determination with parallelisation using GPUs in RELION-2. elife 15:e18722

Kimura Y, Vassylyev DG, Miyazawa A, Kidera A, Matsushima M, Mitsuoka K, Murata K, Hirai T, Fujiyoshi Y (1997) Surface of bacteriorhodopsin revealed by high-resolution electron crystallography. Nature 389:206–211

Kitamura K, Tokunaga M, Iwane AH, Yanagida T (1999) A single myosin head moves along an actin filament with regular steps of 5.3 nanometres. Nature 397:129–134

Li X, Mooney P, Zheng S, Booth CR, Braunfeld MB, Gubbens S, Agard DA, Cheng Y (2013) Electron counting and beam-induced motion correction enable near-atomic-resolution single-particle cryo-EM. Nat Methods 10:584–590

Liao M, Cao E, Julius D, Cheng Y (2013) Structure of the TRPV1 ion channel determined by electron cryo-microscopy. Nature 504:107–112

Llinas P, Isabet T, Song L, Ropars V, Zong B, Benisty H, Sirigu S, Morris C, Kikuti C, Safer D, Sweeney HL, Houdusse A (2015) How actin initiates the motor activity of myosin. Develop Cell 33:401–412

Lymn RW, Taylor EW (1971) Mechanism of adenosine triphosphate hydrolysis by actomyosin. Biochemist 10:4617–4624

Ménétry J, Bahloul A, Wells AL, Yengo CM, Morris CA, Sweeney HL, Houdusse A (2005) The structure of the myosin VI motor reveals the mechanism of directionality reversal. Nature 435:779–785

Ménétry J, Llinas P, Cicolari J, Squires G, Liu X, Li A, Sweeney HL, Houdusse A (2008) The post-rigor structure of the myosin VI and implications for the recovery stroke. EMBO J 27:244–252

Mentes A, Huehn A, Liu X, Zwolak A, Dominguez R, Shuman H, Ostap EM, Sindelar CV (2018) High-resolution cryo-EM structures of actin-bound myosin states reveal the mechanism of myosin force sensing. Proc Natl Acad Sci U S A 115:1292–1297

Mimori Y, Yamashita I, Murata K, Fujiyoshi Y, Yonekura K, Toyoshima C, Namba K (1995) The structure of the R-type straight flagellar filament of Salmonella at 9 Å resolution by electron cryomicroscopy. J Mol Biol 249:69–87

Mitsuoka K, Hirai T, Murata K, Miyazawa A, Kidera A, Kimura Y, Fujiyoshi Y (1999) The structure of bacteriorhodopsin at 3.0 A resolution based on electron crystallography: implication of the charge distribution. J Mol Biol 286:861–882

Miyazawa A, Fujiyoshi Y, Unwin N (2003) Structure and gating mechanism of the acetylcholine receptor pore. Nature 423:949–955

Murata K, Mitsuoka K, Hirai T, Walz T, Agre P, Heymann JB, Engel A, Fujiyoshi Y (2000) Structural determinants of water permeation through aquaporin-1. Nature 407:599–605

Nagy B, Jencks WP (1965) Depolymerization of F-actin by concentrated solutions of salts and denaturing agents. J Am Chem Soc 87:2480–2488

Namba K, Stubbs G (1985) Solving the phase problem in fiber diffraction. Application to tobacco mosaic virus at 3.6A resolution. Acta Crystallogr A41:252–262

Namba K, Stubbs G. (1986) Structure of tobacco mosaic virus at 3.6 Å resolution: implications for assembly. Science 231:1401–1406

Oda T, Iwasa M, Aihara T, Maeda Y, Narita A (2009) The nature of the globular- to fibrous-actin transition. Nature 457:441–445

Otterbein LR, Graceffa P, Dominguez R (2001) The crystal structure of uncomplexed actin in the ADP state. Science 293:708–711

Pollard TD, Borisy GG (2003) Cellular motility driven by assembly and disassembly of actin filaments. Cell 112:453–465

Rayment, I., Rypniewski,W. R., Schmidt-Bäse, K., Smith, R., Tomchick, D. R., Benning, M. M., Winkelmann D. A., Wesenberg, G. & Holden HM. (1993) Three-dimensional structure of myosin subfragment-1: a molecular motor. Science 261, 50–58

Reubold TF, Eschenburg S, Becker A, Kull FJ, Manstein DJ (2003) A structural model for actin-induced nucleotide release in myosin. Nature Struct Biol 10:826–830

Reubold, T. F., Eschenburg, S., Becker, Loonard, M, Schmid, S. L., Vallee, R. B., Kull, F. J. & Manstein, D. J. (2005) Crystal structure of the GTPase domain of rat dynamin 1. Proc Natl Acad Sci U S A 102, 13093–13098

Sachse C, Chen JZ, Coureux P, Stroupe ME, Fandrich M, Grigorieff N (2007) High-resolution electron microscopy of helical specimens: a fresh look at tobacco mosaic virus. J Mol Biol 371:812–835

Samatey FA, Imada K, Nagashima S, Kumasaka T, Yamamoto M, Vonderviszt F, Namba K (2001) Structure of the bacterial flagellar protofilament and implication for a switch for supercoiling. Nature 410:331–337

Samatey FA, Matsunami H, Imada K, Nagashima S, Shaikh TR, Thomas DR, Chen JZ, Derosier DJ, Namba K (2004) Structure of the bacterial flagellar hook and implication for the molecular universal joint mechanism. Nature 431:1062–1068

Scheres SH (2012) RELION: implementation of a Bayesian approach to cryo-EM structure determination. J Struct Biol 180:519–530

Schroder GF, Brunger AT, Levitt M (2007) Combining efficient conformational sampling with a deformable elastic network model facilitates structure refinement at low resolution. Struct 15:1630–1641

Sweeney HL, Houdusse A (2004) The motor mechanism of myosin V: insights for muscle contraction. Philos Trans R Soc B 359:1829–1841

Topf M, Lasker K, Webb B, Wolfson H, Chiu W, Sali A (2008) Protein structure fitting and refinement guided by cryo-EM density. Struct. 16:295–307

von der Ecken J, Heissler SM, Pathan-Chhatbar S, Manstein DJ, Raunser S (2016) Cryo-EM structure of a hyman cytoplasmic actomyosin complex at near-atomic resolution. Nature 354:724–728

Wulf SF, Roparsb V, Fujita-Beckera S, Ostera M, Hofhausa G, Trabucoc LG, Pylypenkob O, Sweeney HL, Houdusseb AM, Schröder R (2016) Force-producing ADP state of myosin bound to actin. Proc Natl Acad Sci U S A 113:E1844–E1852

Yanagida T, Arata T, Oosawa F (1985) Sliding distance of actin filament induced by a myosin crossbridge during one ATP hydrolysis cycle. Nature 316:366–369

Yang Y, Gourinath S, Kovács M, Mitray L, Reutzel R, Himmel DM, O'Neall-Hennessey E, Reshetnikova L, Szent-Györgyi AG, Brown JH, Cohen C (2007) Rigor-like structures from muscle myosins reveal key mechanical elements in the transduction pathways of this allosteric motor. Structure 15:553–564

Yonekura K, Maki-Yonekura S, Namba K (2003) Complete atomic model of the bacterial flagellar filament by electron cryomicroscopy. Nature 424:643–650

Yount RG, Lawson D, Rayment I (1995) Is myosin a "Back Door" Enzyme? Biophys J 68:44s–49s